Journal of Hazardous Materials 159 (2008) 483–491

Contents lists available at ScienceDirect

Journal of Hazardous Materials

journal homepage: www.elsevier.com/locate/jhazmat

# Reductive dechlorination of 3,3′,4,4′-tetrachlorobiphenyl (PCB77) using palladium or palladium/iron nanoparticles and assessment of the reduction in toxic potency in vascular endothelial cells

Karthik Venkatachalam[a], Xabier Arzuaga[b], Nitin Chopra[a], Vasilis G. Gavalas[a], Jian Xu[c], Dibakar Bhattacharyya[c], Bernhard Hennig[b], Leonidas G. Bachas[a,*]

[a] Department of Chemistry, University of Kentucky, Lexington, KY 40506, United States
[b] Molecular and Cell Nutrition Laboratory, College of Agriculture, University of Kentucky, KY 40506, United States
[c] Department of Chemical Engineering, University of Kentucky, Lexington, KY 40506, United States

ARTICLE INFO

*Article history:*
Received 4 May 2007
Received in revised form 16 November 2007
Accepted 18 February 2008
Available online 6 March 2008

*Keywords:*
Palladium nanoparticles
Palladium/iron nanoparticles
Polychlorinated biphenyls
Remediation
Cytotoxicity

ABSTRACT

Palladium-based nanoparticles immobilized in polymeric matrices were applied to the reductive dechlorination of 3,3′,4,4′-tetrachlorobiphenyl (PCB77) at room temperature. Two different dechlorination platforms were evaluated using (1) Pd nanoparticles within conductive polypyrrole films; or (2) immobilized Fe/Pd nanoparticles within polyvinylidene fluoride microfiltration membranes. For the first approach, the polypyrrole film was electrochemically formed in the presence of perchlorate ions that were incorporated into the film to counter-balance the positive charges of the polypyrrole chain. The film was then incubated in a solution containing tetrachloropalladate ions, which were exchanged with the perchlorate ions within the film. During this exchange, reduction of tetrachloropalladate by polypyrrole occurred, which led to the formation of palladium nanoparticles within the film. For the second approach, the membrane-supported Fe/Pd nanoparticles were prepared in three steps: polymerization of acrylic acid in polyvinylidene fluoride microfiltration membrane pores was followed by ion exchange of $Fe^{2+}$, and then chemical reduction of the ferrous ions bound to the carboxylate groups. The membrane-supported iron nanoparticles were then soaked in a solution of tetrachloropalladate resulting in the deposition of Pd on the Fe surface. The nanoparticles prepared by both approaches were employed in the dechlorination of PCB77. The presence of hydrogen was required when the monometallic Pd nanoparticles were employed. The results indicate the removal of chlorine atoms from PCB77, which led to the formation of lower chlorinated intermediates and ultimately biphenyl. Toxicity associated with vascular dysfunction by PCB77 and biphenyl was compared using cultured endothelial cells. The data strongly suggest that the dechlorination system used in this study markedly reduced the proinflammatory activity of PCB77, a persistent organic pollutant.



## 1. Introduction

Because of their interesting properties, polychlorinated biphenyls (PCBs) had been used extensively until their ban in 1979. PCBs can contain 1–10 chlorine atoms leading to 209 possible compounds, called congeners. PCBs are persistent in the environment and can exert toxic effects to animals and humans. The type of toxicity exerted by PCBs depends on their ability to form coplanar structures. Coplanar PCBs, such as those having no chlorine atoms in the *ortho* positions are aryl hydrocarbon receptor (AhR) ligands and can induce CYP1A1 enzymes [1,2]. PCB77 (3,3′,4,4′-tetrachlorobiphenyl) is a coplanar PCB that is commonly found in the environment [3], because of its wide presence in commercial mixtures sold prior to 1979 (e.g., mixtures sold under the trademark Aroclor) [4]. The maximum contaminant level (MCL) for PCBs in drinking water is set by Environmental Protection Agency at 0.5 ppb, and the stated Public Health goal is to reduce the MCL to zero in the future [5]. Thus, significant scientific effort has been directed toward the development of remediation processes for these persistent pollutants [6–8].

The preparation, characterization, and application of metal nanoparticles have been the focus of significant research effort over the past decade [9–11]. The properties of the metal of interest change considerably at nanoscale dimensions owing to differences in both physical and chemical properties [10–13]. These changes in properties lead to interesting applications in the fields of catalysis [9,14,15], energy storage devices [16], optronics [17], magnetic devices [18], and biosensors [19]. The high surface area to

* Corresponding author. Tel.: +1 859 2576350.
*E-mail address:* bachas@uky.edu (L.G. Bachas).

0304-3894/$ – see front matter © 2008 Elsevier B.V. All rights reserved.
doi:10.1016/j.jhazmat.2008.02.109

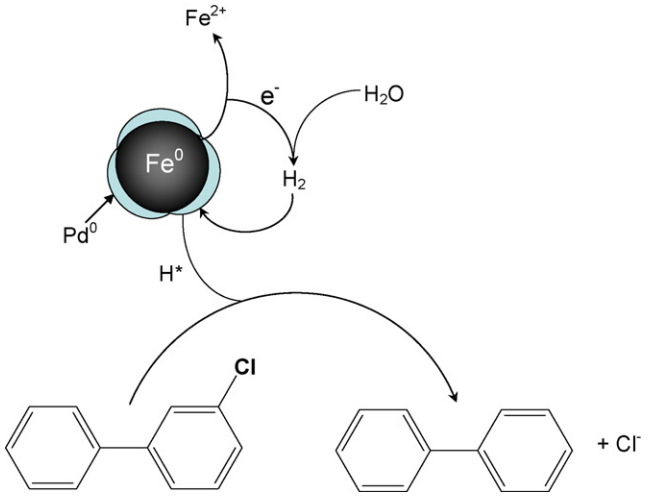


**Scheme 1.** Proposed surface reaction of PCB with Fe/Pd nanoparticles.

volume ratios that nanoparticles exhibit facilitates the effective use of expensive metals in catalysis [11]. Therefore, the creation and development of nanosized materials have brought important and promising techniques into the field of environmental remediation.

Bimetallic catalysis has received much attention because of the significant enhancement in both activity and selectivity at the first and second metal interface [20,21]. The use of nanosized bimetallic particles (e.g., Fe/Ni or Fe/Pd) in the degradation of chlorinated organics has been the focus of several studies in recent years [22–27]. The use of palladium modified bimetallic nanoparticles is particularly important in the treatment of chlorinated aromatics such as PCBs. The role of Pd is to collect $H_2$ generated from the iron corrosion reaction and decompose it into atomic H*, which can be utilized to replace the chlorine in PCBs. (Scheme 1).

In this study, two different platforms were evaluated: (1) immobilized Pd nanoparticles in a polymer matrix using external $H_2$ supply; and (2) immobilized Fe/Pd nanoparticles in membrane matrix without external $H_2$ supply. Both systems employed ion-exchange principles for metal immobilization. In addition, the 2nd platform (Fe/Pd system) can be operated in convective flow mode. For the first approach, a polypyrrole film was electrochemically formed onto a Toray carbon composite paper using chronopotentiometry in the presence of perchlorate. As the polypyrrole film was formed, perchlorate ions were incorporated into the film to counter-balance the positive charges of the polypyrrole chain. These perchlorate ions were exchanged with tetrachloropalladate through incubation of the film in a solution containing tetrachloropalladate ions. During this exchange, palladium nanoparticles were formed into the film, because of the reduction of tetrachloropalladate by polypyrrole. For the preparation of the bimetallic nanoparticles, polymerization of acrylic acid (AA) within the pores of a polyvinylidene fluoride (PVDF) microfiltration membrane was initially performed, followed by ion exchange of $Fe^{2+}$. Chemical reduction of the ferrous ions bound to the carboxylic acid groups resulted in the formation of $Fe^0$ nanoparticles inside the membrane. The palladium layer was formed by immersing the membrane-supported iron nanoparticles in a solution of tetrachloropalladate. This resulted in the deposition of $Pd^0$ on the Fe surface through reduction of $Pd^{2+}$ by the $Fe^0$ nanoparticles. Both systems were evaluated for their ability to dechlorinate PCB77. The results indicate that the final product is biphenyl.

From epidemiological studies, there is substantial evidence that cardiovascular diseases are linked to environmental pollution [28]. For example, a recent study reported increased hospitalization rates for coronary heart disease in populations residing near areas contaminated with persistent organic pollutants such as PCBs [29]. One functional change in cardiovascular diseases, such as atherosclerosis, is the activation of endothelial cells (the inner lining of blood vessels), which is manifested as an increase in the expression of specific cytokines and adhesion molecules. Experiments were performed to determine whether PCB dechlorination leads to formation of products with reduced toxicity to vascular endothelial cells. Accordingly, vascular pulmonary artery-derived endothelial cells were exposed to equimolar concentrations of PCB77 or biphenyl for up to 16 h. After exposure, the relative expression of proteins associated with PCB77-induced inflammation was determined.

## 2. Experimental

### 2.1. Reagents and apparatus

Pyrrole (Sigma–Aldrich, St. Louis, MO) was vacuum distilled prior to use and stored in the dark at −20 °C. $K_2PdCl_4$ (99.99%) was obtained from Alfa Aesar (Ward Hill, MA). PCB77 was obtained from Accustandard (New Haven, CT). PCB calibration standards for the analysis of dechlorinated products were obtained from Ultra Scientific (Northkingstown, RI). All other reagents used were of at least analytical grade. All solutions were prepared using deionized water (Milli-Q water purification system; Millipore, Bedford, MA). This water was autoclaved before preparing the cell culture media.

Electrochemical experiments were performed using a PARSTAT 2273 potentiostat and Powersuite software version 2.40 (EG&G Princeton Applied Research, Princeton, NJ). A Toray carbon composite paper (TCC) working electrode (kind gift from Toray Composites, Tacoma, WA), a silver/silver chloride reference electrode, and a platinum foil counter electrode were used in all electrochemical experiments.

### 2.2. Preparation of nanoparticles

#### 2.2.1. Preparation of Pd nanoparticle

A 200-mL solution containing 0.1 M $KClO_4$ and 0.15 M of freshly distilled pyrrole dissolved in deionized water was transferred to an electrochemical cell consisting of a TCC working electrode (surface area of 8 $cm^2$), an Ag/AgCl reference electrode, and a platinum-foil counter electrode. Chronopotentiometry was performed at a constant current of −5 or −10 mA until 4.5 C/$cm^2$ of charge density was achieved in order to deposit the polypyrrole film onto the TCC. During this process the potential changed from 620 to 735 mV. The formed film was then incubated in a solution of 1 mM potassium tetrachloropalladate in order to form the palladium nanoparticles. Scheme 2 outlines the overall approach.

#### 2.2.2. Preparation of Fe/Pd nanoparticle

The synthesis of membrane based Fe/Pd nanoparticle has been described previously [27]. Briefly, acrylic acid was polymerized within the pores of a polyvinylidene fluoride (PVDF, obtained from Millipore) microfiltration membrane to form sodium polyacrylate (PAA). $Fe^{2+}$ was captured by the PAA-functionalized PVDF membranes by ion-exchange at pH 5.5. Subsequent reduction with $NaBH_4$ (0.07 M) resulted in the formation of $Fe^0$ nanoparticles inside membrane. The membrane-supported iron nanoparticles were then soaked in 50 mL of a solution (90/10 vol% ethanol/water) of $K_2PdCl_4$ (0.12 mM) for 30 min. This resulted in the deposition of Pd on the Fe surface.

### 2.3. Film characterization

In order to visualize the Pd nanoparticles with transmission electron microscopy (TEM), the TCC with the deposited

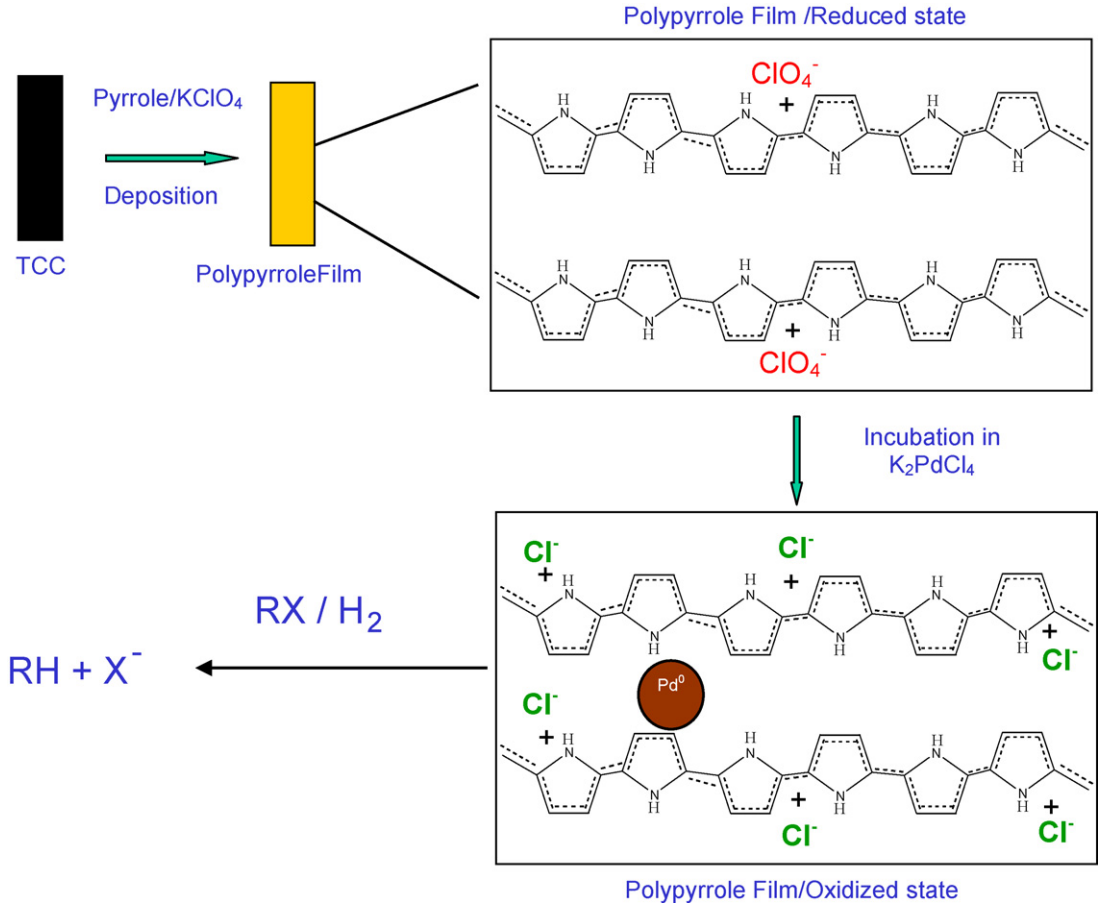


**Scheme 2.** Electrochemical preparation of nanoparticles. Polypyrrole was formed at constant current until 4.5 C/cm$^2$ of current density was achieved from a 0.15 M pyrrole in 0.1 M $KClO_4$ solution. Incubation of the film in 1 mM $K_2PdCl_4$ solution overnight exchanges perchlorate for tetrachloropalladate, which is reduced by polypyrrole to $Pd^0$ in the film. The Pd nanoparticles were used for dechlorination ($RX \rightarrow RH + X^-$) in the presence of hydrogen.

nanoparticles-polypyrrole film was broken into smaller pieces of approximately 5 mm$^2$ and ultrasonicated for 1 min in acetone. The resulting suspension was dropped and air-dried on a 300-mesh gold/copper lacey carbon grid before visualization under the TEM. The Fe/Pd nanoparticle-contained membranes were sectioned with a diamond knife into 50-nm slices using a microtome, and the slices were loaded on a copper TEM grid coated with lacey carbon film. All film samples were characterized using a JEOL-JEM 2010F transmission electron microscope equipped with an Oxford energy dispersive X-ray spectrometer (EDS) and a scanning unit.

Films were also characterized using a Bruker (Madison, WI) D8 Discover X-ray diffractometer (XRD) equipped with a Cu Kα source (1.541 Å). Palladium loading was determined by a Thermo Jarrell Ash ICP-AES system (Franklin, MA) after digesting the film samples in aqua regia with the help of a CEM-MSP 1000 pressure microwave system (Matthews, NC) programmed to hold pressure at 75 psi for 5 min followed by 125 psi for 5 min. All dechlorination products were analyzed using an Agilent GC (Model 6890) fitted with a quadrapole MS detector (Model 5975) (Santa Clara, CA).

### 2.4. Dechlorination experiments

Palladium nanoparticles were used to dechlorinate PCB77 in the presence of hydrogen. All experiments were conducted in 60-mL glass vials, each equipped with a stirrer bar. The polypyrrole film (16.2 cm$^2$) that contained the Pd nanoparticles was added to a 20-mL solution of PCB77 (5 mg L$^{-1}$ in 50% (v/v) ethanol in water). A tube was fitted to the vial to pass hydrogen gas from a regulated cylinder at 10 psi. Dechlorination experiments were conducted for 2, 4, or 6 h. After the dechlorination experiments, the solution was extracted with 5 mL hexane for 12 h in a wrist-action shaker to attain extraction equilibrium. Additionally, the polypyrrole film was extracted with 10 mL hexane for 12 h in order to retrieve products absorbed into the film.

The dechlorination efficiency of the Fe/Pd nanoparticles was evaluated using a 15.6 mg/L PCB77 in 65% (v/v) ethanol in water with Fe/Pd (Pd: 2.3 wt%) immobilized inside a PVDF/PAA polymer membrane (0.22 (m pore size, 4.7 cm diameter, 125 (m thickness). The PCB77 degradation experiments were conducted in 24.5-mL glass vials capped with Teflon-lined silicon septa. A 4.7-cm in diameter PAA/PVDF membrane loaded with 16 mg Fe/Pd nanoparticles was placed in each vial that contained a 20-mL solution of PCB77, and the solution was agitated using a wrist-action shaker. At predetermined time intervals, PCB77 and its breakdown products were extracted with hexane from a 2-mL aliquot of the reaction mixture. At the end of the reaction 10 mL of hexane was added to extract residual starting material and products from the membrane phase. Both extractions were performed using a wrist-action shaker.

### 2.5. Analysis of dechlorinated products

GC–MS was employed to analyze the dechlorination products. A volume of 100 μL of the extract was placed in a 2-mL GC autosampler vial fitted with a polymer inset, which could hold a volume of 150 μL. Ten microliters of 1 mg L$^{-1}$ PCB209 was added as an internal

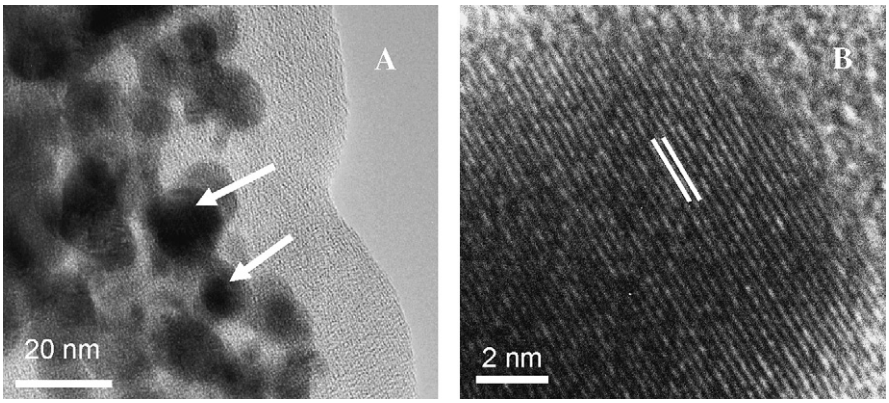


**Fig. 1.** (A) TEM of polypyrrole film with $Pd^0$ nanoparticles of $14 \pm 2$ nm diameter. Two nanoparticles are marked by arrows. (B) High resolution image showing the lattice plane of the Pd fcc structure.

standard. Standards of PCB77 and dechlorinated products in hexane were used to prepare calibration plots.

### 2.6. Cell culture

Endothelial cells were isolated from porcine pulmonary arteries and cultured as described previously [30]. Porcine arteries were donated from the College of Agriculture, University of Kentucky. Cells were sub-cultured in Medium 199 containing 10% (v/v) fetal bovine serum (FBS, HyClone Laboratories, Logan, UT) using standard techniques [30]. When the cells reached 100% confluency, the cell culture medium was switched from 10 to 1% FBS. After 8 h in the 1% FBS containing medium, the cells were treated with variable concentrations of PCB77 or biphenyl (0.01–1 μM) for 18 h. The treatment solutions were prepared by adding PCB77 or biphenyl from a stock solution in DMSO to 1% (v/v) FBS medium. All treatment solutions contained an equal amount of DMSO. The final DMSO concentration in the experiment did not exceed 0.05% (v/v) in all treatment groups.

### 2.7. Measurement of VCAM-1, COX-2, and CYP1A1 protein expression

Cellular protein extraction was performed as described previously [31]. Cell monolayers were harvested and washed in cold phosphate buffer saline, pelleted and incubated in lysis buffer containing 20 mM Tris, 150 mM NaCl, 1 mM EDTA, 0.5 mM dithiothreitol (DTT), 0.5 mM phenylmethanesulfonyl fluoride (PMSF), 1 mg $L^{-1}$ leupeptin, 1 mg $L^{-1}$ pepstatin, 0.1% (v/v) Nonidet P-40, and 0.5% (w/v) Triton X-100, pH 7.5. Protein extracts were electrophoresed on 12% SDS-polyacrylamide gels and transferred to nitrocellulose membranes. Proteins were probed with commercial rabbit and goat antibodies for VCAM-1, COX-2, and CYP1A1 (Santa Cruz Biotechnology, Santa Cruz, CA), and β-actin (rabbit polyclonal IgG, Sigma, St. Louis, MO). β-Actin was used for normalizing the expression of proteins of interest. Antibodies were diluted 1:1000 in blocking buffer (5% (w/v) non-fat dry milk in Tris buffered saline with Tween-20 (TBST-milk) or in Tris buffered saline (TBS-milk), pH 7.4). Secondary HRP-linked antibodies were purchased from Santa Cruz Biotechnology or Cell Signaling (Danvers, MA) and diluted 1:3000 in blocking buffer. Blots were developed using an Image Station 2000R (KODAK Molecular Imaging Systems, New Haven, CT) using ECL (GE Healthcare, Piscataway, NJ) for chemiluminescence detection. Experiments were performed in triplicate. Sigmastat (Systat Software, San Jose, CA) was used for statistical analysis. Treatment comparisons were made by one-way ANOVA, and Tukey tests were used for post-hoc comparisons. A statistical probability of $p < 0.05$ was considered significant.

## 3. Results and discussion

### 3.1. Pd nanoparticle characterization

Nanoparticles have been incorporated into polypyrrole using both electrochemical and chemical methods [32–39]. Polypyrrole has positive charges in its fully oxidized form for every 3–4 pyrrole units and can be doped with anions to compensate this charge [40]. Various studies have shown that neutral and doped polypyrrole can incorporate palladium from acidic aqueous $PdCl_2$ solutions where $[PdCl_4]^{2-}$ is the dominant species [36,38]. Hasik et al. [36] noted that the initial dopant anion ($Cl^-$ or $OH^-$) as well as the pH conditions influences the way palladium species are incorporated into polypyrrole.

In this study, palladium nanoparticles were incorporated into polypyrrole by exchanging the dopant ions (perchlorate) with tetrachloropalladate. During this exchange, palladium nanoparticles were formed into the film, because of the reduction of tetrachloropalladate by polypyrrole. Released chloride ions stay in the membrane to counterbalance the polypyrrole positive charge. Fig. 1A shows the resulting Pd nanoparticles on a 300-mesh gold/copper lacey carbon grid under a TEM equipped with an EDS detector (two of the nanoparticles are marked with arrows). High resolution TEM images of the Pd particles (Fig. 1B) showed the lattice planes of the Pd fcc structure confirmed by the lattice spacing of 0.225 nm for the [1 1 1] plane [41]. EDS demonstrated that the nanoparticles are composed of palladium (Fig. 2). The diameter of the particles was found to be $14 \pm 2$ nm ($n = 50$).

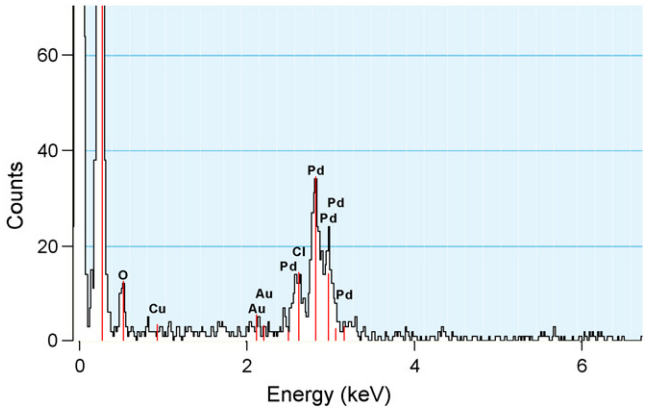


**Fig. 2.** EDS of the film after incorporation of $Pd^0$ nanoparticles into the polypyrrole film. The Au and Cu signals are from the TEM grid.

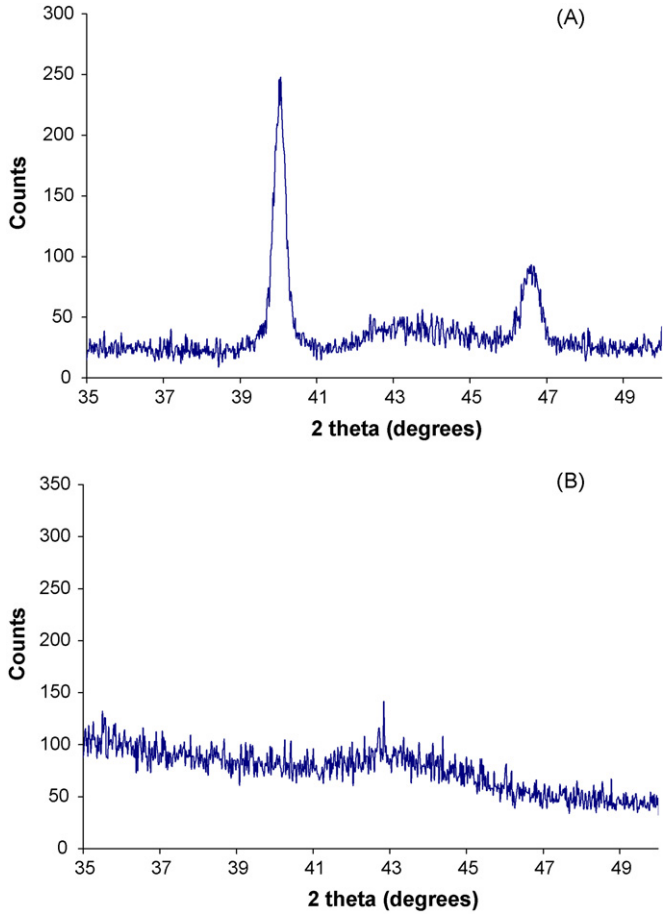


**Fig. 3.** (A) XRD of polypyrrole film after exposure to tetrachloropalladate solution, which leads to reduction of $Pd^{2+}$ to $Pd^0$ within the film and (B) XRD of polypyrrole film before exposure to tetrachloropalladate solution.

X-ray diffraction (XRD) was employed to investigate the nature of the entrapped palladium into the polypyrrole films. The XRD pattern of $Pd^0$ contains characteristic peaks at 40.1° and 46.6° [41]. Analysis of the polymer films before and after deposition of Pd confirmed that the nanoparticles formed after the polypyrrole film doped with perchlorate ions was incubated with tetrachloropalladate ions. The presence of peaks corresponding to the 1 1 1 lattice plane ($2\theta = 40.1°$) and 2 0 0 lattice plane ($2\theta = 46.6°$) of $Pd^0$ were observed in the film after it was incubated in a $K_2PdCl_4$ solution (Fig. 3A). These peaks were absent in the polypyrrole film doped with perchlorate ions (Fig. 3B). Additionally no peaks were observed at $2\theta = 36.0°$ (Fig. 3A) corresponding to $Pd^{2+}$ of the tetrachloropalladate ion, indicating the absence of this ion in the film. The particle size of the palladium nanoparticles was calculated to be 17 nm using the Scherrer equation and is slightly different from the size determined by TEM ($14 \pm 2$ nm). Similar discrepancies in size have been reported previously [34], and are attributed to the fact that large crystalline domains (i.e., larger nanoparticles) dominate the signal in XRD.

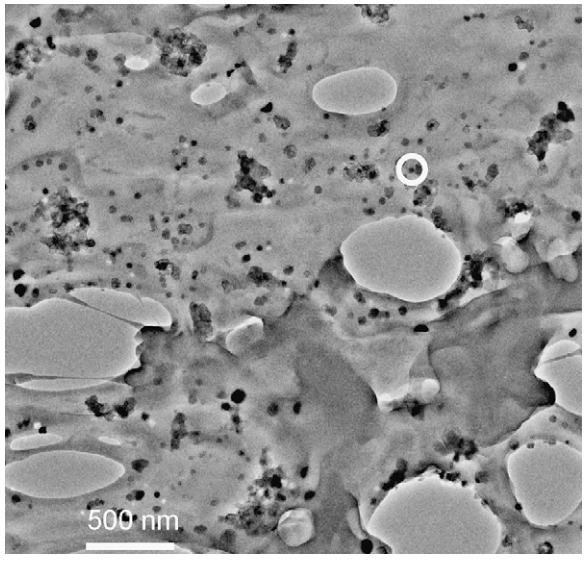


**Fig. 4.** STEM mode imaging of PAA/PVDF membrane cross-section containing Fe/Pd nanoparticles confirmed by XRD. One such particle is marked by the white circle.

Palladium loading was determined by ICP-AES. Polypyrrole film samples were subjected to pressure microwave digestion using aqua regia. The results showed that the film contained $9.6 \pm 0.1$ μmol of Pd per $cm^2$ of film ($n = 3$). This value was used in calculations involving evaluation of the kinetic parameters.

### 3.2. Fe/Pd nanoparticle characterization

Transmission electron microscopy analysis (Fig. 4) indicates a dispersion of spherical shaped Fe/Pd nanoparticles with an average particle diameter of $30 \pm 6$ nm over the entire membrane. Our previous studies using STEM-EDS mapping showed a clear core–shell structure of Fe/Pd (iron in the core region and palladium in the shell region) [27]. Based on the diameter of 30 nm, the surface area of the nanoparticles was calculated to be 25 $m^2\ g^{-1}$.

### 3.3. Dechlorination efficiency

Both platforms were evaluated for their dechlorination efficiency. In the experiments with the Pd nanoparticles, external supply of hydrogen is required to achieve dechlorination. In the bimetallic Fe/Pd system, the chlorinated organics are reduced to non-chlorinated hydrocarbons on the palladium surface by highly active hydrogen species and electrons generated at the Fe/Pd interface from the $Fe^0$ corrosion reaction (Scheme 1). Thus, no external hydrogen supply is required in the Fe/Pd system. The possible intermediates following dechlorination of PCB77 are shown in Scheme 3.

Fig. 5A shows the concentration profiles for the dechlorination reaction of PCB77 with the palladium nanoparticles in the polypyrrole film. Around 85% of PCB77 was dechlorinated within 2 h with 0.82 g $L^{-1}$ of palladium nanoparticle loading. PCB77 was ultimately converted to biphenyl and only small amounts of the intermediates were detected. Fig. 5A also shows carbon mass balance data calculated from the concentrations of PCB77 and each dechlorination product at different reaction times. Carbon balance values ranged from 88 to 99% of the theoretically expected value, and the difference corresponds to mass losses during the extraction process. Fig. 5B depicts the dechlorination of PCB 77 with the Fe/Pd nanoparticles immobilized inside the PAA/PVDF polymer membrane matrix. Complete dechlorination of PCB77 by Fe/Pd in the PAA/PVDF membrane was achieved within 2 h. Again, biphenyl was formed as the main dechlorination product. The carbon mass balance in this case was on average about ~95% of the initial amount of PCB77.

In both cases, the degradation of PCB77 by the Pd or the Fe/Pd nanoparticles occurred through the formation of less chlorinated intermediates. It has been proven in the literature [25] that non-*ortho*-chlorinated PCB congeners dechlorinate faster than the *ortho*-chlorinated isomers. The reactivity of the chlorine substituents decreases in the order *para* ≈ *meta* > *ortho* [42]. The degradation for PCB77 with both platforms showed all eight intermediates, which can occur in theory under reductive dechlorination. All the intermediates appeared at very low concentration

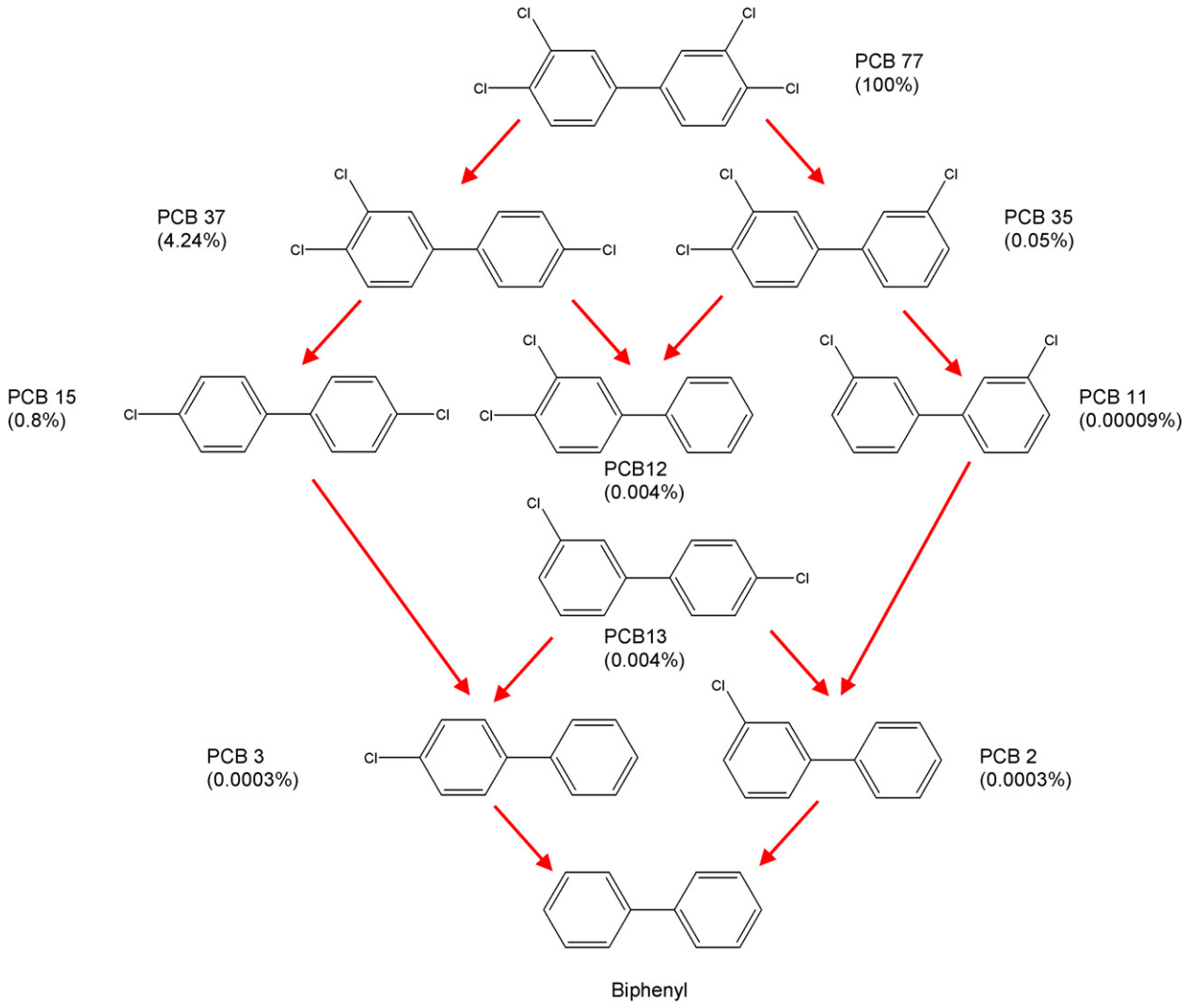


**Scheme 3.** Dechlorination pathway of PCB77 leading to lower chlorinated biphenyls and ultimately biphenyl. The values in parenthesis indicate relative toxicities (with PCB77 assigned a toxicity of 100%) calculated according to the model in ref. [45].

levels. This can be explained by the little difference of reactivity between *para* and *meta* chlorines substituents.

It is well known that pseudo-first-order kinetics can be used to describe PCB dechlorination with nanoparticles [25–27]. This was found to be applicable to the bimetallic Fe/Pd nanoparticles and is a good approximation for the dechlorination reaction using Pd nanoparticles in the presence of excess hydrogen. Thus, the dechlorination kinetics of both platforms can be described by the following equation:

$$-\frac{dC}{dt} = k_{obs}C = k_{SA}\rho_m a_S C \quad (1)$$

where $C$ is the PCB77 concentration, $a_S$ is the surface area of the nanoparticles ($m^2\,g^{-1}$), $\rho_m$ is the loading of the nanoparticles, $k_{obs}$ is the observed rate constant ($h^{-1}$), and $k_{SA}$ is the surface-area-normalized rate constant ($L\,h^{-1}\,m^{-2}$). For the Pd nanoparticles, based on the average diameter of 14 nm (identified by TEM), $a_S$ was calculated to be $36\,m^2\,g^{-1}$. The experimental data were fitted to Eq. (1) to obtain the kinetic parameters $k_{obs}$ and $k_{SA}$, which were found to be $0.58\,h^{-1}$ and $0.019\,L\,h^{-1}\,m^{-2}$, respectively. Similarly, for the 30 nm in diameter Fe/Pd nanoparticles the $k_{obs}$ and $k_{SA}$ were determined to be $2.82\,h^{-1}$ and $0.141\,L\,h^{-1}\,m^{-2}$, respectively. These results indicate that the Fe/Pd nanoparticles are ~7-fold more efficient in the dechlorination of PCB77. The higher $k_{SA}$ for the Fe/Pd system can be explained by the in-situ hydrogen generation at the Fe/Pd interface, which can minimize the hydrogen transfer resistance to the Pd surface. The electrons generated by iron corrosion could also benefit the PCB dechlorination. In the pure Pd (with Pd/polypyrrole) system, $H_2$ needs to be dissolved in the aqueous phase and then transferred to the Pd surface by diffusion, and thus may lower the observed reaction rate due to mass-transfer resistance.

During dechlorination with the Fe/Pd nanoparticles, the iron is oxidized, and $Fe^{2+}/Fe^{3+}$ species may be released from the membrane. The PAA-functionalized membrane could capture these dissolved iron ions. Analysis of the aqueous phase after the dechlorination reaction showed negligible amount of iron (0.03 mg, which corresponds to 0.18 wt% of initial iron). In order to measure iron ions in the membrane phase, ion exchange with $Ba^{2+}$ was performed to transfer iron ions captured by the PAA from the membrane phase to the aqueous phase. Analysis of the aqueous phase after $Ba^{2+}$ ion exchange showed 1.2 mg iron (2% of the initial Fe) captured by membrane.

### 3.4. Toxicity

Coplanar PCBs such as PCB77 bind to and activate the aryl hydrocarbon receptor (AhR). Most of the toxic effects caused by

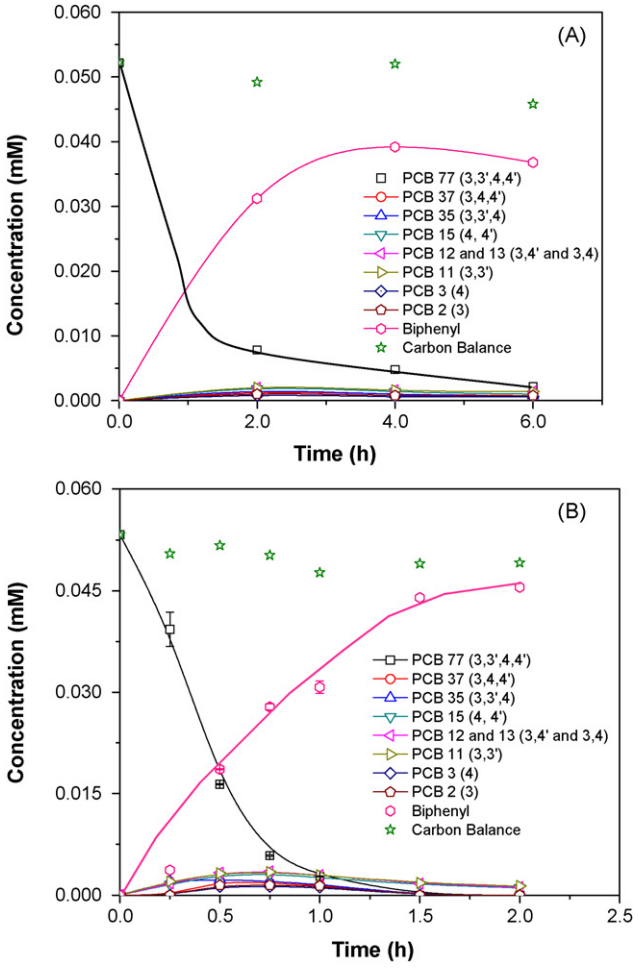


**Fig. 5.** Concentration profiles of PCB77, dechlorinated product intermediates, biphenyl, and the corresponding carbon balance. (A) Batch reaction of PCB77 with Pd nanoparticles in polypyrrole membrane in the presence of excess $H_2$. (B) Batch reaction of PCB77 with Fe/Pd nanoparticles in PAA/PVDF membrane.

coplanar PCBs in vascular endothelial cells are mediated by the AhR [43,44]. The relative toxicity of PCB77 and its lower chlorinated biphenyl intermediates formed during dechlorination can be calculated using computational approaches based on the affinity of these compounds for the aryl hydrocarbon receptor [45]. The relative toxicity calculated by this approach is shown in Scheme 3 assigning PCB77 a relative toxicity value of 100%. The values indicate that the dechlorination intermediates have significantly lower toxicity. Because only small amounts of chlorinated intermediates are generated during the dechlorination process (Fig. 5), the toxicity of biphenyl (main product) was evaluated in order to assess the dechlorination process.

There is mounting evidence that exposure to environmental pollutants, especially to persistent chlorinated organic compounds such as PCBs, can play a critical role in the pathology of cardiovascular diseases. Dysfunction of the endothelial lining of blood vessels is a critical underlying cause for the initiation of cardiovascular diseases. Thus, vascular endothelial cells were chosen as the target organ for toxicity studies. Endothelial cells were exposed for 16 h to PCB77 or biphenyl. Expression of CYP1A1, COX2, VCAM-1, and β-actin was measured by western blot analysis. CYP1A1 induction is a commonly used biomarker of exposure to chlorinated and non-chlorinated AhR ligands. Exposure to coplanar PCBs such as PCB77 activates the AhR, which results in increased expression of CYP1A1 mRNA, and the corresponding CYP1A1 protein [43]. Previous studies have demonstrated that PCB-dependent induction of endothelial cell toxicity is mediated by AhR activation and induction of responsive genes [43,44]. As shown in Fig. 6, CYP1A1 protein expression was induced by PCB77 in a dose-dependent fashion, but not by biphenyl. The lack of induction of CYP1A1 in endothelial cells after exposure to biphenyl suggests that this chemical does not activate the AhR pathway and its responsive genes.

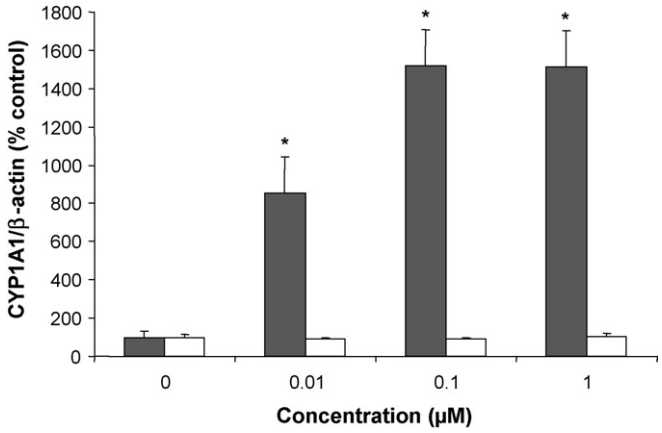


**Fig. 6.** Effect of PCB77 (black bars) and biphenyl (white bars) on CYP1A1 protein expression. CYP1A1 protein expression was normalized to β-actin expression and converted to % control. Bars represent mean ± standard error; $n = 3$ cell culture plates per treatment. * indicates statistically significant difference with respect to the vehicle (DMSO) treatment.

COX-2 expression has been associated with oxidative stress [46] and the formation of early atherosclerotic lesions in LDL receptor deficient mice (a mouse research model commonly used to study atherosclerosis) [47]. COX-2 can be induced by chlorinated (e.g., PCBs and dioxins) and non-chlorinated AhR ligands in various cell culture models [48,49]. Induction of COX-2 by AhR ligands has been shown to be dependent on activation of AhR and the pro-inflammatory transcription factor nuclear factor-kappa B (NF-κB) [49–51]. COX-2 protein expression was induced by PCB77 in a dose-dependent fashion, but not by biphenyl (Fig. 7). These results suggest that biphenyl is unable to activate AhR and NF-κB at the doses used in these experiments. The PCB77 treatment also caused

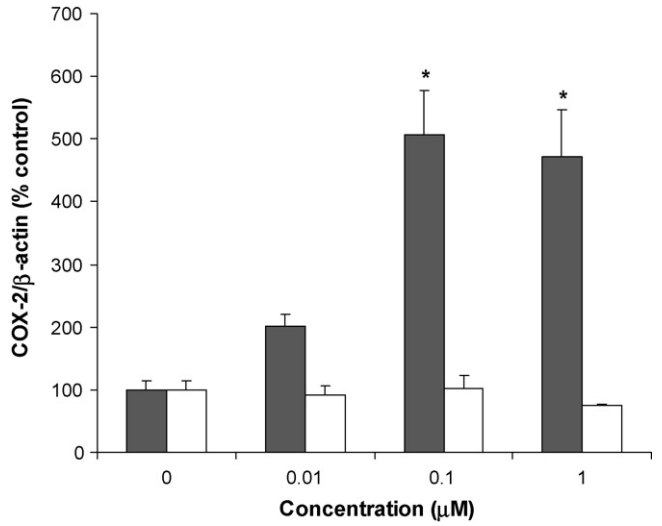


**Fig. 7.** Effect of PCB77 (black bars) and biphenyl (white bars) on the expression of COX-2 protein. COX-2 protein expression was normalized to β-actin expression and converted to % control. Bars represent mean ± standard error; $n = 3$ cell culture plates per treatment. (*) indicates statistically significant difference with respect to the vehicle (DMSO) treatment.

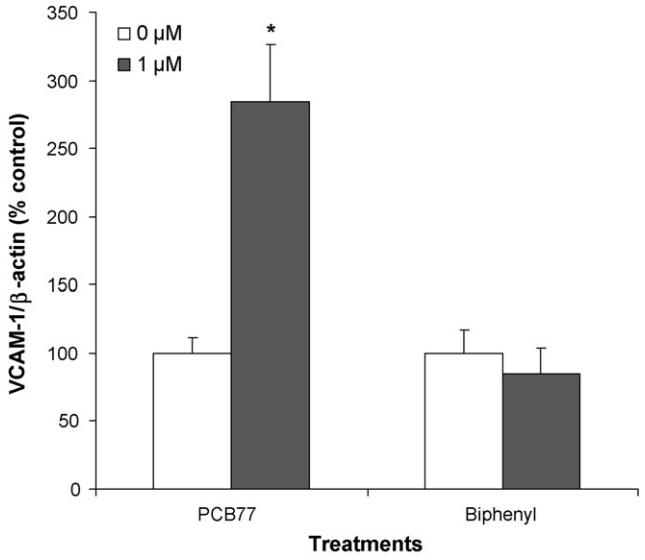


**Fig. 8.** Effect of PCB77 and biphenyl at 0 and 1 μM concentration on the expression of VCAM-1 protein. VCAM-1 protein expression was normalized to β-actin expression and converted to % control. Bars represent mean ± standard error; $n = 3$ cell culture plates per treatment. (*) indicates statistically significant difference with respect to the vehicle (DMSO) treatment.

an increase in VCAM-1 protein expression, which was not observed in endothelial cell cultures treated with biphenyl (Fig. 8). These findings are significant and confirm our previous studies, which demonstrate proinflammatory properties of PCBs [43].

Our studies with biphenyl demonstrate a lower toxicity than PCB77 in an endothelial cell system at concentrations less than 1 μM. It should be noted, however, that biphenyl may demonstrate toxic effects at concentrations higher than those investigated in this study.

## 4. Conclusions

Reductive dechlorination of conjugated aromatics can be accomplished through the use of Pd in the reactive media. Two different Pd based platforms were evaluated, i.e., Pd nanoparticles immobilized in polypyrrole membranes using external $H_2$ supply, and Fe/Pd bimetallic nanoparticles in polyacrylate-polyvinylidene fluoride microfiltration membranes without external $H_2$ supply. The membranes were characterized by TEM, EDS and XRD techniques to determine and confirm the size and nature of the incorporated nanoparticles. The bimetallic nanoparticles exhibit higher reactivity in terms of kinetics for the dechlorination of PCB77. At the same time, toxicity results suggest that biphenyl (the dechlorination end-product), unlike PCB77, does not activate the AhR pathway and does not alter expression of proteins associated with vascular inflammation. This implies a reduction in endothelial cell toxicity upon treatment of PCB77 solutions with Pd or Fe/Pd nanoparticles.

## Acknowledgements

This publication was made possible by grant number P42 ES 07380 from the National Institute of Environmental Health Sciences (NIEHS), NIH. Its contents are solely the responsibility of the authors and do not necessarily represent the official views of the NIEHS, NIH. The authors thank Toray Composites America, Tacoma, WA for providing Toray carbon composite paper, and Larry W. Robertson for providing PCB77 for the cell culture experiments.

## References

[1] P. Pocar, T.A. Brevini, S. Antonini, F. Gandolfi, Cellular and molecular mechanisms mediating the effect of polychlorinated biphenyls on oocyte in vitro maturation, Reprod. Toxicol. 22 (2006) 242–249.
[2] J.P. Giesy, K. Kannan, Dioxin-like and non-dioxin-like toxic effects of polychlorinated biphenyls (PCBs): implications for risk assessment, Crit. Rev. Toxicol. 28 (1998) 511–569.
[3] D.G. Patterson Jr., G.D. Todd, W.E. Turner, V. Maggio, L.R. Alexander, L.L. Needham, Levels of non-*ortho*-substituted (coplanar), mono- and di-*ortho*-substituted polychlorinated biphenyls, dibenzo-*p*-dioxins, and dibenzofurans in human serum and adipose tissue, Environ. Health Perspect. 102 (Suppl. 1) (1994) 195–204.
[4] N. Kannan, S. Tanabe, T. Wakimoto, R. Tatsukawa, Coplanar polychlorinated biphenyls in Aroclor and Kanechlor mixtures, J. Assoc. Off. Anal. Chem. 70 (1987) 451–454.
[5] EPA, National Primary Drinking Water Standards EPA Publication 816-F-03-016, 2003, available online at http://www.epa.gov/safewater/consumer/pdf/mcl.pdf.
[6] J.M. Tiedje, T.V. Tsoi, K.D. Pennell, L.D. Hansen, A. Wani, D.P. Howell, Enhancing PCB bioremediation, in: J.W. Talley (Ed.), Bioremediation of Recalcitrant Compounds, CRC Press, Boca Raton, FL, 2006, pp. 147–214.
[7] V. Birke, J. Mattik, D. Runne, Mechanochemical reductive dehalogenation of hazardous polyhalogenated contaminants, J. Mater. Sci. 39 (2004) 5111–5116.
[8] S.K. Lee, A. Mills, Detoxification of water by semiconductor photocatalysis, J. Ind. Eng. Chem. 10 (2004) 173–187.
[9] D. Astruc, F. Lu, J.R. Aranzaes, Nanoparticles as recyclable catalysts: the frontier between homogeneous and heterogeneous catalysis, Angew. Chem., Int. Ed. 44 (2005) 7852–7872.
[10] G. Schmid, Metals, in: K.J. Klabunde (Ed.), Nanoscale Materials in Chemistry, Wiley-Interscience, New York, NY, 2001, pp. 15–59.
[11] J.H. Fendler, Y. Tian, Nanoparticles and nanostructured films: current accomplishments and future prospects, in: J.H. Fendler (Ed.), Nanoparticles and Nanostructured Films: Preparation, Characterization and Applications, Wiley-VCH, Weinheim, Germany, 1998, pp. 429–461.
[12] M.M. Alvarez, J.T. Khoury, T.G. Schaaff, M.N. Shafigullin, I. Vezmar, R.L. Whetten, Optical absorption spectra of nanocrystal gold molecules, J. Phys. Chem. B 101 (1997) 3706–3712.
[13] B.M. Quinn, P. Liljeroth, V. Ruiz, T. Laaksonen, K. Kontturi, Electrochemical resolution of 15 oxidation states for monolayer protected gold nanoparticles, J. Am. Chem. Soc. 125 (2003) 6644–6645.
[14] S. Kidambi, M.L. Bruening, Multilayered polyelectrolyte films containing palladium nanoparticles: synthesis, characterization, and application in selective hydrogenation, Chem. Mater. 17 (2005) 301–307.
[15] Y. Niu, L.K. Yeung, R.M. Crooks, Size-selective hydrogenation of olefins by dendrimer-encapsulated palladium nanoparticles, J. Am. Chem. Soc. 123 (2001) 6840–6846.
[16] P.V. Kamat, Meeting the clean energy demand: nanostructure architectures for solar energy conversion, J. Phys. Chem. C 111 (2007) 2834–2860.
[17] J.H. Park, Y.T. Lim, O.O. Park, J.K. Kim, J.W. Yu, Y.C. Kim, Polymer/gold nanoparticle nanocomposite light-emitting diodes: enhancement of electroluminescence stability and quantum efficiency of blue-light-emitting polymers, Chem. Mater. 16 (2004) 688–692.
[18] K. Yakushiji, F. Ernult, H. Imamura, K. Yamane, S. Mitani, K. Takanashi, S. Takahashi, S. Maekawa, H. Fujimori, Enhanced spin accumulation and novel magnetotransport in nanoparticles, Nat. Mater. 4 (2005) 57–61.
[19] J.S. Ye, A. Ottova, H.T. Tien, F.S. Sheu, Nanostructured platinum–lipid bilayer composite as biosensor, Bioelectrochemistry 59 (2003) 65–72.
[20] B. Coq, F. Figueras, Structure-activity relationships in catalysis by metals: some aspects of particle size, bimetallic and supports effects, Coord. Chem. Rev. 178–180 (Pt 2) (1998) 1753–1783.
[21] M.O. Nutt, K.N. Heck, P. Alvarez, M.S. Wong, Improved Pd-on-Au bimetallic nanoparticle catalysts for aqueous-phase trichloroethene hydrodechlorination, Appl. Catal. B 69 (2006) 115–125.
[22] C. Grittini, M. Malcomson, Q. Fernando, N. Korte, Rapid dechlorination of polychlorinated biphenyls on the surface of a Pd/Fe bimetallic system, Environ. Sci. Technol. 29 (1995) 2898–2900.
[23] W.X. Zhang, C.B. Wang, H.L. Lien, Treatment of chlorinated organic contaminants with nanoscale bimetallic particles, Catal. Today 40 (1998) 387–395.
[24] N.E. Korte, O.R. West, L. Liang, B. Gu, J.L. Zutman, Q. Fernando, The effect of solvent concentration on the use of palladized-iron for the step-wise dechlorination of polychlorinated biphenyls in soil extracts, Waste Manage. 22 (2002) 343–349.
[25] G.V. Lowry, K.M. Johnson, Congener-specific dechlorination of dissolved PCBs by microscale and nanoscale zerovalent iron in a water/methanol solution, Environ. Sci. Technol. 38 (2004) 5208–5216.
[26] F. He, D. Zhao, J. Liu, C.B. Roberts, Stabilization of Fe–Pd nanoparticles with sodium carboxymethyl cellulose for enhanced transport and dechlorination of trichloroethylene in soil and groundwater, Ind. Eng. Chem. Res. 46 (2007) 29–34.
[27] J. Xu, D. Bhattacharyya, Fe/Pd nanoparticle immobilization in microfiltration membrane pores: synthesis, characterization, and application in the dechlorination of polychlorinated biphenyls, Ind. Eng. Chem. Res. 46 (2007) 2348–2359.

[28] B. Hennig, E. Oesterling, M. Toborek, Environmental toxicity, nutrition, and gene interactions in the development of atherosclerosis, Nutr. Metab. Cardiovasc. Dis. 17 (2007) 162–169.
[29] A.V. Sergeev, D.O. Carpenter, Hospitalization rates for coronary heart disease in relation to residence near areas contaminated with persistent organic pollutants and other pollutants, Environ. Health Perspect. 113 (2005) 756–761.
[30] M. Toborek, Y.W. Lee, S. Kaiser, B. Hennig, Measurement of inflammatory properties of fatty acids in human endothelial cells, Methods Enzymol. 352 (2002) 198–219.
[31] R. Slim, M. Toborek, L.W. Robertson, B. Hennig, Antioxidant protection against PCB-mediated endothelial cell activation, Toxicol. Sci. 52 (1999) 232–239.
[32] K. Venkatachalam, V.G. Gavalas, S. Xu, A.C. de Leon, D. Bhattacharyya, L.G. Bachas, Poly(amino acid)-facilitated electrochemical growth of metal nanoparticles, J. Nanosci. Nanotechnol. 6 (2006) 2408–2412.
[33] L. Li, E.T. Kang, K.G. Neoh, Preparation of conductive polypyrrole–palladium composite nanospheres by inverse microemulsion polymerization, J. Nanosci. Nanotechnol. 6 (2006) 2571–2575.
[34] M. Sigaud, M. Li, S. Chardon-Noblat, F.J.C. Santos Aires, Y. Soldo-Olivier, J.P. Simon, A. Renouprez, A. Deronzier, Electrochemical preparation of nanometer sized noble metal particles into a polypyrrole functionalized by a molecular electrocatalyst precursor, J. Mater. Chem. 14 (2004) 2606–2608.
[35] K.M. Mangold, F. Meik, K. Juttner, Polypyrrole/palladium composites for the electrocatalyzed Heck reaction, Synth. Met. 144 (2004) 221–227.
[36] M. Hasik, A. Bernasik, A. Adamczyk, G. Malata, K. Kowalski, J. Camra, Polypyrrole–palladium systems prepared in $PdCl_2$ aqueous solutions, Eur. Polym. J. 39 (2003) 1669–1678.
[37] N. Cioffi, L. Torsi, L. Sabbatini, P.G. Zambonin, T. Bleve-Zacheo, Electrosynthesis and characterization of nanostructured palladium–polypyrrole composites, J. Electroanal. Chem. 488 (2000) 42–47.
[38] S.W. Huang, K.G. Neoh, E.T. Kang, H.S. Han, K.L. Tan, Palladium-containing polyaniline and polypyrrole microparticles, J. Mater. Chem. 8 (1998) 1743–1748.
[39] S.W. Huang, K.G. Neoh, C.W. Shih, D.S. Lim, E.T. Kang, H.S. Han, K.L. Tan, Synthesis, characterization and catalytic properties of palladium-containing electroactive polymers, Synth. Met. 96 (1998) 117–122.
[40] G.G. Wallace, P.C. Innis, Inherently conducting polymer nanostructures, J. Nanosci. Nanotechnol. 2 (2002) 441–451.
[41] International Centre for Diffraction Data, Powder Diffraction File (PDF) number 46-1043.
[42] Y. Noma, M. Ohno, S. Sakai, Pathways for the degradation of PCBs by palladium-catalyzed dechlorination, Fresenius Environ. Bull. 12 (2003) 302–308.
[43] B. Hennig, P. Meerarani, R. Slim, M. Toborek, A. Daugherty, A.E. Silverstone, L.W. Robertson, Proinflammatory properties of coplanar PCBs: in vitro and in vivo evidence, Toxicol. Appl. Pharmacol. 181 (2002) 174–183.
[44] P. Ramadass, P. Meerarani, M. Toborek, L.W. Robertson, B. Hennig, Dietary flavonoids modulate PCB-induced oxidative stress, CYP1A1 induction, and AhR-DNA binding activity in vascular endothelial cells, Toxicol. Sci. 76 (2003) 212–219.
[45] S.A. Kafafi, H.Y. Afeefy, A.H. Ali, H.K. Said, I.S. Abd-Elazem, A.G. Kafafi, Affinities for the aryl hydrocarbon receptor, potencies as aryl hydrocarbon hydroxylase inducers and relative toxicities of polychlorinated biphenyls. A congener specific approach., Carcinogenesis 14 (1993) 2063–2071.
[46] J.A. Leopold, J. Loscalzo, Oxidative enzymopathies and vascular disease, Arterioscler. Thromb. Vasc. Biol. 25 (2005) 1332–1340.
[47] M.E. Burleigh, V.R. Babaev, J.A. Oates, R.C. Harris, S. Gautam, D. Riendeau, L.J. Marnett, J.D. Morrow, S. Fazio, M.F. Linton, Cyclooxygenase-2 promotes early atherosclerotic lesion formation in LDL receptor-deficient mice, Circulation 105 (2002) 1816–1823.
[48] D. Wolfle, S. Marotzki, D. Dartsch, W. Schafer, H. Marquardt, Induction of cyclooxygenase expression and enhancement of malignant cell transformation by 2,3,7,8-tetrachlorodibenzo-*p*-dioxin, Carcinogenesis 21 (2002) 15–21.
[49] Z. Yan, K. Subbaramaiah, T. Camilli, F. Zhang, T. Tanabe, T.A. McCaffrey, A.J. Dannenberg, B.B. Weksler, Benzo[*a*]pyrene induces the transcription of cyclooxygenase-2 in vascular smooth muscle cells. Evidence for the involvement of extracellular signal-regulated kinase and NF-kappaB, J. Biol. Chem. 275 (2000) 4949–4955.
[50] A. Puga, A. Hoffer, S. Zhou, J.M. Bohm, G.D. Leikauf, H.G. Shertzer, Sustained increase in intracellular free calcium and activation of cyclooxygenase-2 expression in mouse hepatoma cells treated with dioxin, Biochem. Pharmacol. 54 (1997) 1287–1296.
[51] M.W. Weng, Y.M. Hsiao, C.J. Chen, J.P. Wang, W.C. Chen, J.L. Ko, Benzo[*a*]pyrene diol epoxide up-regulates COX-2 expression through NF-kappaB in rat astrocytes, Toxicol. Lett. 151 (2004) 345–355.